J MATER SCI **41** (2006) 2121–2131

Damage and loading rate effects on the microfailure behaviour of Al_2O_3-ceramics studied by SEM

V. N. KYTOPOULOS, G. A. PAPADOPOULOS
Department of Engineering Science, Section of Mechanics, The National Technical University of Athens, 5, Heroes of Polytechnion Avenue, GR-157 73 Zographou, Athens, Greece

T. SADOWSKI
Technical University of Lublin, Nadbystrzycka 36 Street, PL-20-618 Lublin, Poland

Published online: 17 February 2006

A scanning electron microscopy (SEM)-X-ray combined experimental approach to qualitative and semi-quantitative characterization of microfailure behaviour of an Al_2O_3-ceramic material in terms of induced damage is presented. The qualitative approach was based on representative fractographical images and data obtained by SEM whereas the semi-quantitative approach was based on a new technique of the X-ray electron probe microanalysis (X-ray EPMA) capable to detect the localized subsurface damage. The damage was induced by a simple rotary notch-cutting procedure where the associated damage parameters can be controlled by the cutting rate. By correlating certain characteristic macro- and microfractographic features/patterns with well-known microfailure mechanisms it was possible to make qualitatively, in an indirect way, evident the existence of induced damage which was assumed to be ideal brittle having only microcracking component. In the same correlating way the stimulating effect of internal pores on the damage development was deduced. Observed loading rate effects on the fractographic behaviour expressed by changes in fracture roughness and micromorphology were attributed to pore-assisted microcracking linkage. Low porosity under high loading rates tends to lower the fractographic roughness, a fact which can be related with a reduction in the ability of energy dissipation. On the other hand, high porosity under increasing loading rates leads to non observable changes in the fractographic roughness, a fact which is indicative of corresponding no appreciable changes in the dissipative character of the material. The measured local damage distribution ahead of the notch-tip shows a monotonic increasing of damaging effects toward the tip. By means of this distribution the total or average damage degree and process zone length ahead of the notch-tip were evaluated. The increase of these two damage parameters is not proportional to the increase in the cutting speed i.e. the rate of damage development. Finally, by assuming brittle damage an experimental approaching procedure for the estimation of the induced energy required for the microcracking damage was proposed.

1. Introduction

Aluminum oxide-based ceramic is widely used as an engineering material for example in ceramic-metal composites referred to as cerments. Such composites find extensive commercial use as insert tips for hard metal-cutting. Furthermore, the composite with ZrO_2-particles embedded within a Al_2O_3 matrix presents a significant high fracture toughness which is related to phenomena of dissipation of a portion of the energy available for fracture because of the stress induced martensitic transformation. However, significant increases in fracture toughness (K_I) have been obtained with dispersed-phase composites, but only in systems such as Al_2O_3/SiC where alumina matrix has a relative low fracture toughness. This is attributed mainly to the complex brittle fracture of that matrix under different loading rates in which many occurring microfailure mechanisms are not yet well understood. In this context we should mention, for example, the complex microfail-

0022-2461
DOI: 10.1007/s10853-006-3638-z

ure behaviour of long-fibre composites where the failure mode is that of progressive, time-dependent, load transfer mechanism from already micro-cracked matrix followed by fibre fracture and pull-put. In general, the model response of similar composites to an applied stress is first elastic extension (stage I) until micro-cracking begins in the matrix and progressive load-transfer to the fibres optimally aligned with the stress axis occurs (stage II) followed by fibre pull-out from the micro-cracked matrix (stage III). From the above mentioned the importance of the micro-cracking stress as well as the matrix fracture energy or toughness concerning the stage II and in general the microfailure behaviour of the matrix may become evident [1, 2]. Hence, further elucidation of the micro-cracking behaviour of the matrix material under different loading rates plays a very important role in the toughness improvement in such composites. In this direction one of most simple and most used experimental techniques is for example the micro-hardness test referred to as the strength or controlled flaw test (CFT) in which the indentation is used as a controlled flaw or precrack. Especially, the damage zone, controlling the residual stresses, is selected as primary variable to be studied for Al_2O_3-ceramics and other materials [2–5]. So, at the same time the problem of evaluation of such damage zones i.e. micro-cracking fields arises. In solving this problem the (mechanical) damage could be operatively divided in two main types: surface, (visible) and subsurface or internal damage. The first type of damage is an important parameter in fatigue loading, where as it is know the micro-cracking generally starts from the material surface, whereas the second type plays an important role for example in creep loading [6]. To date there are many macroscopic and microscopic techniques for the large and small-scale damage evaluation [6–19]. Among the microscopic ones those which can detect localized subsurface damage in the material play a special role because they are best developed and mostly applied in fatigue testing to establish correlations between microstructure and mechanical properties. At this instance it must be pointed out that most of the above microscopic techniques are imaging ones by which a direct quantitative or a semi-quantitative assessment of the local damage is possible only with special computer programming. Furthermore, the use of many of the above cited methods is "restricted" as to the type of material [7, 14, 15, 18, 19].

The purpose of the present work is three fold. First, to try to find by means of electron fractography some new qualitative correlations between certain fracture micromechanisms and mechanical or microstructural parameters of the ceramic material concerning its microfailure behaviour under various damage and loading rates effects. Second, to try by means of the X-ray electron probe microanalysis technique to introduce a new semi-quantitative experimental approach to the local damage distribution, total (average) degree of damage and the process zone size (length). Third, to introduce an experimental approach by which the two damage parameters (average damage degree and process zone length) can be controlled by a "rotating disc-cutting procedure" where at the same time the damaging notch is introduced. Such "damage-controlled" techniques would be useful for example for experimental verification of damage-dependent constitutive models [6, 8]. It is expected that this technique will be developed in the near future for complementary material characterization in terms of fracture toughness.

2. Experimental procedure

Polycrystalline alumina powder which contained 0.5–1.0% MgO, was used by compression sintering to prepare orthogonal specimen plates in dimensions of $0.1 \times 0.015 \times 0.004$ m with porosity of 6% and 33%. Some specimens were used for the three-point slow bending tests. Other specimens were prepared to be used in the Charpy test, which is assumed to simulate a dynamic three-point bending behaviour. Small specimens were cut from the above plates to study in the SEM the cutting-induced damage in front of the notch-tip. The notches were introduced by a diamond cutting disc of 0.0001 m thickness and in this manner the width of the notches was 0.00013 m. The lowest rotary cutting speed was chosen to be S1 as one arbitrary unit and so another higher speed was given for example by $S3 = 3 \times S1$ three times of S1. The duration of cutting was one minute and the applied load 5 N. The cutting procedure was carried out by means of a cutting device of a Buehler-Isomet type designed for high precision specimen preparation. Where mechanical distortions of the material can be minimized.

The fractographical data for the qualitative approach in this study were obtained by means of a Scanning Electron Microscope of type S4-10. The specimens were fractured and then "post-mortem" examined in the SEM. Before examination the specimens were coated by vacuum evaporation with a thin gold layer to avoid electron charging effects which can lead to a degradation of the image quality and at the same time to increase the emission of secondary electrons. Despite the applied conducting layer such charging effects were observed at magnifications higher than about $1000\times$ and hence higher magnifications could not be used.

The semi-quantitative approach concerning the local damage measurements was performed by means of a wave-length dispersive X-ray micro-analyzer, of a Microspec WDX-210 type, attached to SEM. Concerning this micro-analysis procedure, some further experimental details will be given in the respective section about the damage estimation in the following text.

3. Results and discussion

3.1. Fractographical approach

The following topofractographical approach concerns a qualitative study where relating quantitative parameters such as roughness, waviness or fractal dimension have not been measured.

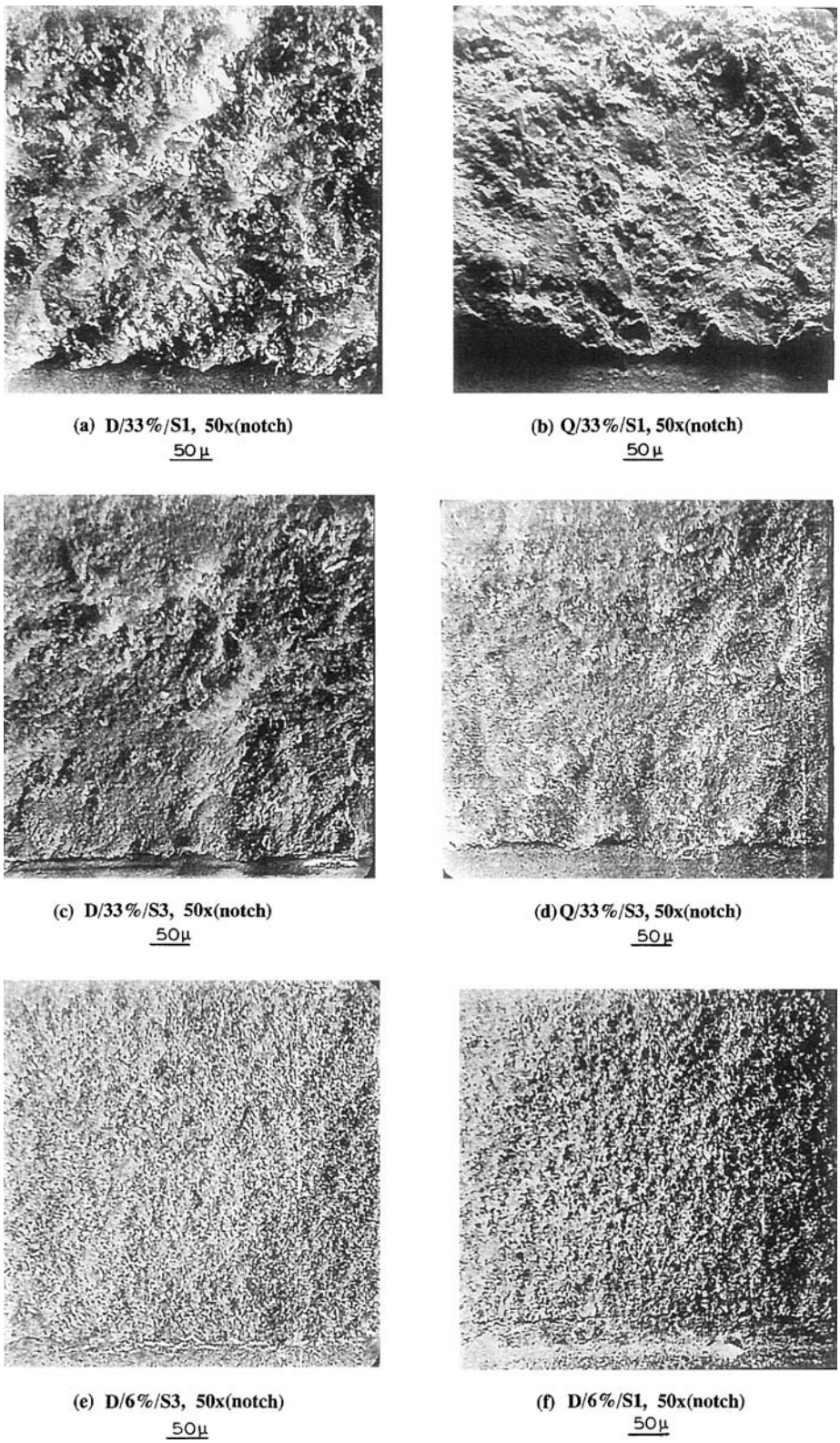

Figure 1 SEM-photographs showing the macrofractographic behaviour of specimen surfaces on large-scale level at low magnification (50×), for 33% Porosity, impact loading "*D*"(a, c), three point bending "*Q*" (b, d) and operative damage level *S*1 (a, b) and *S*3 (=3×*S*1) (c, d). (Direction of crack propagation from bottom to top. Machined (smooth) part of the notch edge is seen at bottom, and photographed surface area $\approx 2 \times 2\,\text{mm}^2$).

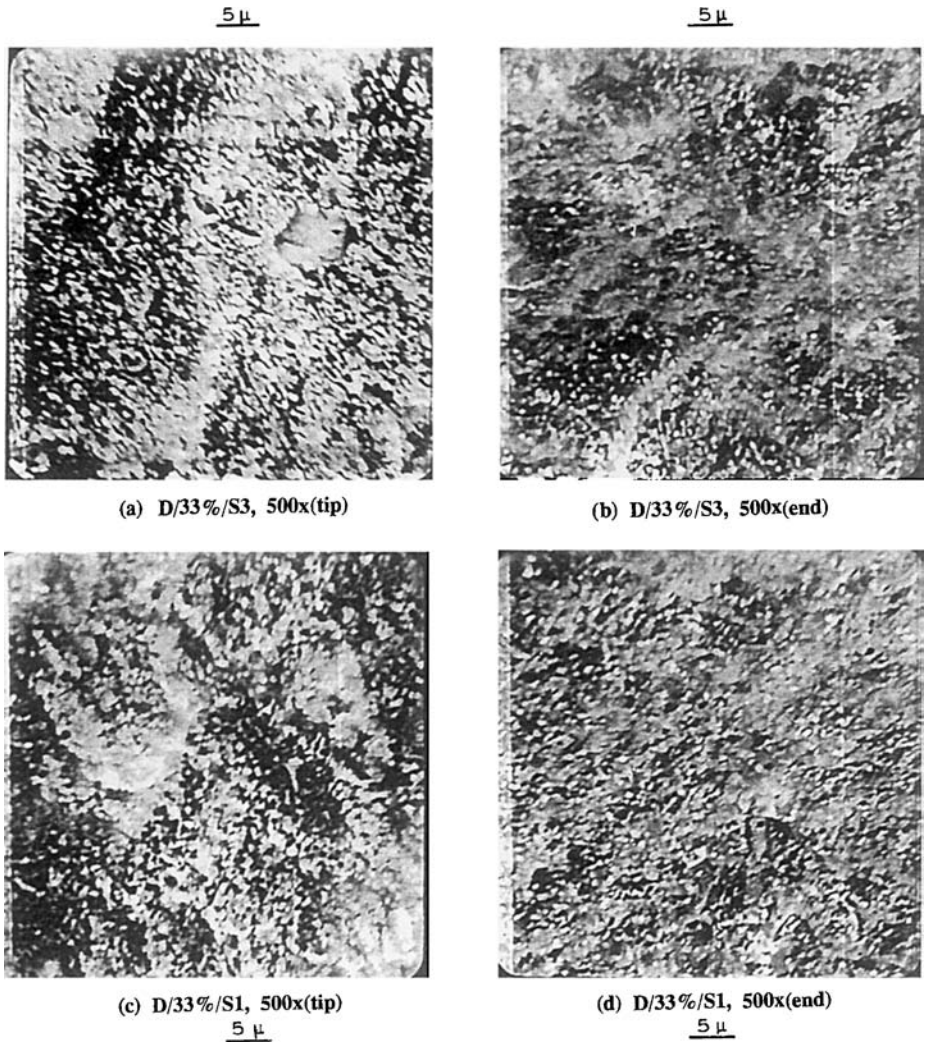

Figure 2 SEM-photographs showing the microfractographic behaviour of specimen surfaces on small-scale or micro-level (at higher magnification 500×), for 33% Porosity impact loading "*D*", and operative damage level *S*3 (a, b) and *S*1 (c, d). "Pitting" pattern formation is observed in (a) and (c). (Direction of crack propagation from bottom to top. Photographed surface area = $200 \times 200\,\mu m^2$. Bottom edge of photographs *a*, *c* coincides with notch edge and top edge of *b*, *d* with ending edge of fracture surface).

Certain qualitative SEM-informations about fracture surfaces for several ceramic specimens are presented in the series of photographs of Figs 1–3. The characteristics of the specimens are given by a "triplet" of characters, for example "*D*/6%/S1" which means dynamic loading (impact Charpy) *D*, percent of porosity 6% and the low speed of cutting wheel S1.

The series of photographs in Fig. 1 shows the large-scale effect of the induced damage and that of the loading rate (dynamic (*D*) and quasi-static (*Q*)) on the fracture topography for specimens with 33% porosity. For example by comparing the photographs (a) with (c) and (b) with (d) we can see macrofractographically the effect of the increasing cutting speed to reduce the surface roughness. This could be explained by the fact that the increased localized damage, induced mainly in form of intergranular microcracks due to the increase in the cutting speed, by interaction with clustered pores may act as combined-defect sites for crack initiation. It is assumed that high porosity may locally act as clustered pores or pore-cluster formation. Moreover and according, to reference [15], a so called "mirror"-like "area" is formed around such sites as fracture origin. In our case "mirror-like microareas" are formed around these sites during the cutting process. During the fracture test and due to high triaxial notch stress field these microareas can link to form larger "mirror-like areas" which on large-scale level appear as smoothed surface with reduced average roughness. Reduction in surface roughness is indicative of associated reduction in the fracture energy i.e. the dissipation ability of the material and in this sense the induced damage should have tendency in lowering the fracture toughness. Furthermore by comparing the photographs (a) with (b) and (c) with (d) it can be deduced that the change in the loading rate from quasi-static to dynamic has negliable influence on the macromorfology of the fracture surface and hence on the average roughness. As mentioned before, because of the high porosity intergranular microcrack-like defects

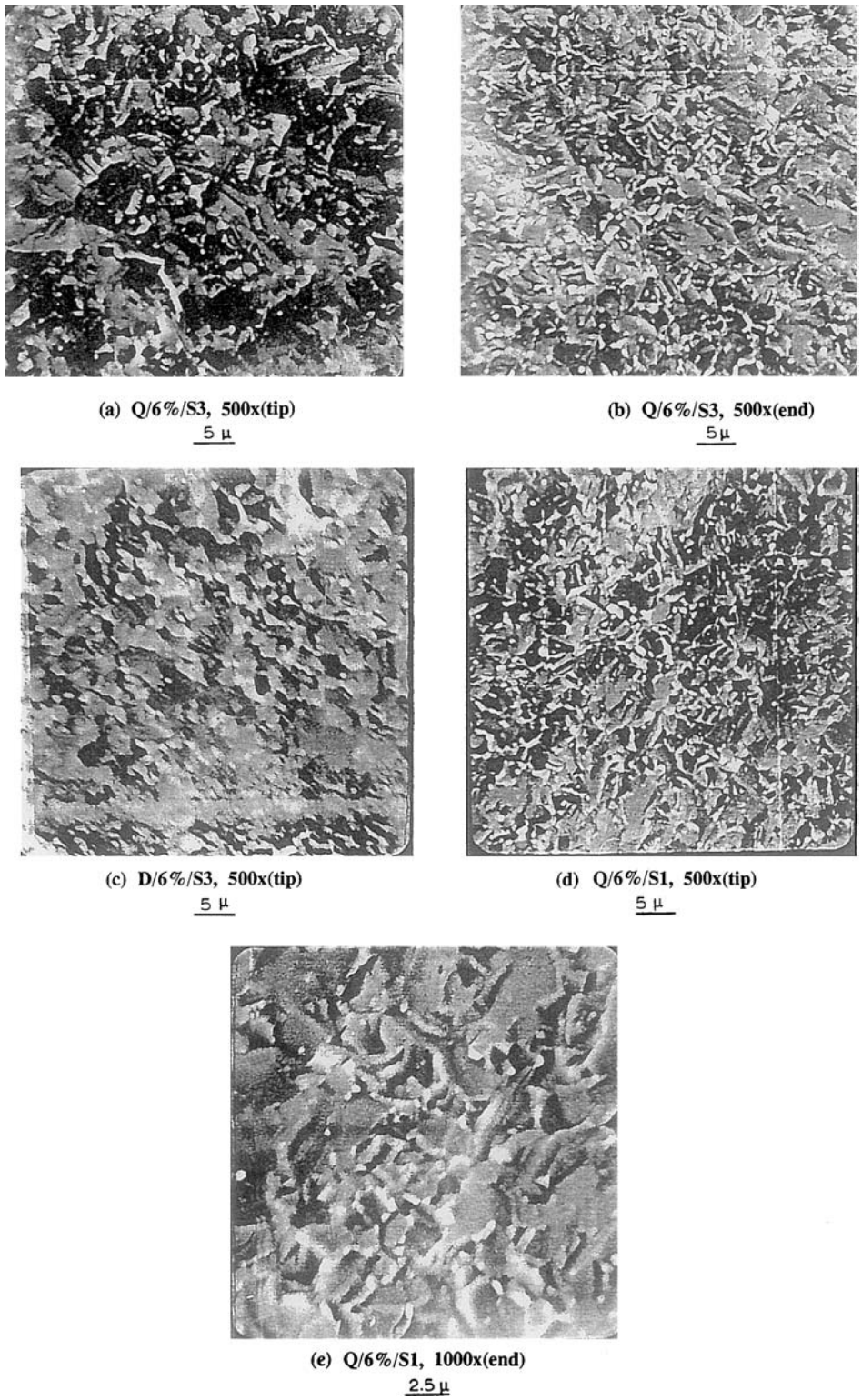

Figure 3 SEM-photographs showing the microfractographic behaviour of specimen surfaces on grain boundary level (at higher magnification 500×) for 6% Porosity, impact loading "*D*" (c), three-point bending "*Q*" (a, b, d) and operative damage level *S*1 (d) and *S*3 = (3 × *S*1) (a, b, c). (Direction of crack propagation from bottom to top. Photographed surface area ≈ 200 × 200 μm^2. Bottom edge of photographs *a*, *c*, *d* coincides with notch edge and top edge of (b) and (e) with ending edge of fractured surface.

are developed around clustered pores which now act as a "combined-defects" sites for initiation of crack propagation [18]. These sites are "optimal large-sized" to have effectively enough time to link under high loading rates and so to give a similar net effect as it would be for a linkage under low loading rates.

The series of photographs in Fig. 2, taken at higher magnification compared to photographs of Fig. 1, shows

the "small-scale effect" of the induced damage on the morphology of the fractured surface. By closer examination of photographs (a) and (c) we can distinguish certain "pitting" pattern formation. (The "white" local regions and vertical "white band" in photographs are due to electron charging effects despite the conductive thin metal layer which was prior deposited by evaporation coating). Furthermore, this "pitting pattern" formation occurs mainly near the notch tip, Fig 2a and c, and to a much lower extent further away i.e. at the end of the fracture surface as shown in Fig 2b and d. So it can be argued that such "pattern" is an indirect evidence of the intergranular microcracking damage induced at the notch-root as a resultant of micromechanical interactions processes which promote clustered pores-microcrack damaging sites formation. The subsequent crack propagation leads to a linkage of such "combined-defect" sites by forming "super-cavities" which in turn microfractographically i.e. on small-scale level appear as "pits".

The series of photographs in Fig. 3 shows the fracture surface micromorphology developed at grain level of specimens with 6% porosity. By comparing Fig. 3a with b one can roughly deduce the prevailing intergranular failure mode in the first, at notch tip, and transgranular one in the second, at the end of the fractured surface. In this case because of the much lower porosity the micromechanical processes determined by single pore-microcrack interactions may promote the formation of "combined" defect sites localized between grains and along grain boundaries. The local linkage of such "combined-defect" sites leads to a intergranular weakening followed by dominating intergranular crack propagation and in this sense Fig. 3a can by regarded as another indirect evidence of the introduced intergranular damage at the notch-root. Furthermore, loading rate seems to has an influence on the micro-failure behaviour of specimens with low porosity (6%). This can be deduced by comparing photographs (a) and (c) in Fig. 3 where high loading rates, due to a more transgranular or mixed mode of micro-failure, tend to lower the apparent roughness of the fractured surface. This could be explained by the fact that under high loading rates there is no enough time for linkage of the "small-sized" single pore-microcrack damaging sites and thus for the formation of an intergranular crack propagation path. At the same time a lower portion of the total fracture energy should be spent for the formation of a dominant transgranular crack propagation path which from its inherent nature of initiation require lower energies compared to that of intergranular path [20]. The exact conditions for transition from transgranular to intergranular failure (and viceversa) are not yet fully understood and hence require further investigations [19, 20].

Furthermore, by comparing the photographs (a) with (d) in Fig. 3 one can deduce the effect of the increase in the introduced operative damage (S1 to S3) on the microfailure behaviour on grain scale level. Especially, a low degree of induced operative damage (denoted by S1 in Fig. 3d) leads to a more mixed mode whereas a higher degree of operative damage (denoted by S3 in Fig. 3a) to a more intergranular mode of crack propagation. It seems that an increase in the cutting speed, under influence of low porosity, tends to improve the materials' ability of energy dissipation and hence to increase the absorbed fracture energy.

Finally, by inspection of photographs (d) and (e) the effect of the notch-tip triaxial state on the fracture can be distincted. Triaxial state (photograph-c) shows a dominating intergranular propagation mode compared to the end of fractured surface (photograph e) which slows a dominating transgranular mode.

3.2. Semi-quantitative approach to damage estimation

In the previous section (A) of this paper concerning the qualitative approach to the microfailure behaviour the relative strong effect of the cutting-induced microcracking damage in changing the roughness of the fractured surface and thus in fact to affect the absorbed or dissipated fracture energy has been shown. Thus, as it was mentioned in the introduction it would be of great importance to be able to estimate or evaluate locally by any other complementary way this damage. In this sense a novel technique for a relative estimation of the degree of brittle damage ahead of a notch (crack) in Alumina specimens is presented. The ratio of cutting speeds, was used as an operational parameter for the control of the rate of the induced damage.

3.2.1. Basic theoretical considerations

During inelastic scattering of the beam electrons in the solid specimen, two kinds of X-rays are generated: continuous X-rays and characteristic X-rays [20]. Depending on the critical excitation energy, certain characteristic X-rays are generated over a substantial material volume fraction of the interaction of the electron beam with the solid. In order to predict the depth of X-ray production (penetration), the electron penetration range also called electron range, must be known. The problem of defining the electron range is analyzed elsewhere [20]. Based on experimental results concerning the X-ray production and electron range, Andersen and Hasler [20] developed the so called mass-range equation for X-ray production, which is the most widely used in the respective literature

$$\rho R_x = 0.064\left(E_0^{1.7} - E_c^{1.7}\right) = \text{const.} \qquad (1)$$

where ρ is the mass density of the solid, R_x is the measure of the depth of X-ray generation (in μm), E_0 is the operating voltage on the SEM (in KV) and E_c is the critical excitation energy (in KV) for a given characteristic X-ray wavelength for the element in the solid. For example, taking for a fully dense Alumina solid $\rho_0 \cong 4$ gr/cm^2 and E_0=40 KV as a maximum operating voltage and $E_c^{\mathrm{Al\,(Ka)}} = 1,5$ KV, from Equation 1 we obtain

$R_x \cong 8\,\mu$m. If E_0 and E_c are constants, from Equation 1 we can also obtain

$$\rho_0 R_x = \tilde{\rho}\tilde{R}_x = \text{const.} \tag{2}$$

where $\tilde{\rho}$ and $\tilde{R}_x$ are new parameters for a micro-cracking damaged fully dense Alumina solid and $\tilde{\rho} < \rho_0$ and $\tilde{R}_x > R_x \cong 8\,\mu$m is the minimum detection range (depth). (the index "x" refers to X-ray).

Taking now into consideration a "real" Alumina material, with finite amount of porosity, the relation (2) becomes

$$\rho_0 R_x = \tilde{\rho}\tilde{R}_x = \tilde{\tilde{\rho}}_i \tilde{\tilde{R}}_{xi} = \text{const.} = c_x \tag{2a}$$

where $\tilde{\tilde{\rho}}_i$ is the mass density of the damaged porous material and $\tilde{\tilde{R}}_{xi}$ is the corresponding X-ray generation depth. If now, $i = 1, 2, 3, \ldots$ is an indicator number for the increasing damage degree, then from the above statements it is easy to deduce the inequalities:

$$\begin{aligned} &4\ \text{g/cm}^3 > \rho_0 > \tilde{\rho} > \tilde{\tilde{\rho}}_1 > \tilde{\tilde{\rho}}_2 > \cdots > \tilde{\tilde{\rho}}_i \ \text{and/or} \\ &8\mu\text{m} \le R_x < \tilde{R}_x < \tilde{\tilde{R}}_{x1} < \tilde{\tilde{R}}_{x2} < \cdots < \tilde{\tilde{R}}_{xi}. \end{aligned} \tag{2b}$$

It is obvious that for a damaged solid the depth of X-ray generation is increased but, at the same time, it is well known that the emitted X-ray intensity is lowered by strong (exponential) absorption effects due to the increase in path length of travelling, i.e. in depth R_x of generation [22]. It can be deduced that in this way we can have some information about the damaged material from a depth greater than that of about 8 μm.

There are certain principles of applying from the existing micro-and macroscopic damage measures the most adequate one to define and to quantify material damage [6, 8]. The latter is characterized by the development of distributed microscopic cavities and/or microcracks in materials leading to the deterioration of their mechanical properties. The mechanical variables which describe such damage states should not have only a physical meaning but also should have proper physical and mathematical properties. From the above it can be deduced that most adequate damage measure for our problem might be a macroscopic one described by the material's mass density (ρ) as a mechanical variable.

Furthermore, the total emitted X-ray intensity from a given sampling point 'i' is given by the equation [22, 23]:

$$I_{\text{em}}^{(i)} = \int_0^{c_x} \Phi(\rho z) \exp\left[-\frac{\mu}{\rho} t(\rho z)\right] d(\rho z) \tag{2c}$$

where $t(\rho z) = \rho z \csc\psi \cdot \sin(90^\circ - \vartheta)$ is an effective mass range or "mass path length" over which X-rays can be absorbed in the sample, z is a depth dimension, μ/ρ the local mass absorption coefficient, ψ the take-off angle, ∂ the tilt angle and $\Phi(\rho z)$ the depth distribution function of generated X-rays. The integration in the above equation is performed from the surface, $\rho z = 0$, to the position $\rho z = \rho R_x = c_x$ where the x-rays are not longer generated. During the surface sampling procedure we have $\psi = \vartheta = \text{const.} = 45^\circ$. Also, the shape of the depth distribution $\Phi(\rho z)$ don't alter because it depends only on the atomic number Z and the constant parameters E_0 and E_c [22]. A formal integration of Equation 2c leads to a more simple and general form: $I_{\text{em}}^{(i)} = \tilde{I}(\mu_i/\tilde{\tilde{\rho}}_i)$ which means that the emitted intensity must be a function of local mass absorption coefficient ($\tilde{\tilde{\rho}}_i$ has the meaning given by the relations (2b)). Taken into consideration (Equation 2c) we can establish the basic inequality: $I_{\text{em}}^{(i)} \rangle\langle I_{\text{em}}^{(k)}$ for the condition $\mu_i/\tilde{\tilde{\rho}}_i \rangle\langle \mu_k/\tilde{\tilde{\rho}}_k$. Furthermore (Equation 2c) may be simulated by a "infinite" number of Beer- type absorption processes which means that any increase (decrease) in the emitted intensity must be attributed in a first instance to a corresponding decrease (increase) in the linear absorption coefficient, μ. This fact leads to the supplementary condition $\mu_i \rangle\langle \mu_k$. By dividing this last condition with $\tilde{\tilde{\rho}}_i\tilde{\tilde{\rho}}_k$ we obtain $(\frac{\mu_i}{\tilde{\tilde{\rho}}_i})\frac{1}{\tilde{\tilde{\rho}}_k} \rangle\langle (\frac{\mu_k}{\tilde{\tilde{\rho}}_k})\frac{1}{\tilde{\tilde{\rho}}_i}$ and by multiplying this with the assumed density relation $\tilde{\tilde{\rho}}_i \rangle\langle \tilde{\tilde{\rho}}_k$ we obtain finally the above given condition $\mu_i/\tilde{\tilde{\rho}}_i \rangle\langle \mu_k/\tilde{\tilde{\rho}}_k$. In this case the assumed density relation is valid which means that during the sampling procedure across the surface any increase (decrease) in the measured X-ray intensity must be attributed to a corresponding increase (decrease) in the local density of the material.

3.2.2. Experimental estimation of damage degree and process zone length

From the above statements one can expect variations of the detected X-rays due to changes in the $\tilde{\tilde{\rho}}_i$, i.e. actual mass density of the real solid (specimen with 6% porosity). The electron probe of the scanning electron microscope can be easily chosen so as to have optimal spatial resolution. In this manner we can detect local or very localized variations in the X-ray signal and so corresponding changes in the local mass density which are connected with changes in the micro-cracking field.

For this purpose, we have used the technique of the electron probe microanalysis (EPMA) which was performed by means of a WDX-210 microspec unit, attached to the SEM. The description of this kind of units is given elsewhere [22, 23]. For the sake of completeness, we must point out the following basic experimental precautions:

(1) Specimens positioning along the z-axis (electron beam axis) are only required to be in a range about ± 0.5 mm to obtain reproducible data. This range enables us to scan and to sampling the specimen in the

desired range without difficulties and without specimen topographical influences.

(2) Small variations in the emitted X-rays and thus corresponding very small subsurface variations in the local mass density $\tilde{\tilde{\rho}}_i(x)$, i.e. in the micro-cracking field, can be detected by displaying the mean input rate in the Ratemeter unit on a greatly expanded scale in the linear ranges by means of a variable zero suppression control (DC-offset). In this manner background or other information below the region of interest is offset by this control and, by switching to a lower range, any fluctuations in the X-ray count rate are displayed on a much larger scale.

(3) The geometrical parameters such as inclination of the local surface to the incident beam and the take-off angle to the X-ray detector can vary very little due to very small scanned areas. In this manner, the effective depth from which X-rays are emitted doesn't alter.

Now, in Fig. 4a the sketch of the expected general form of the X-ray signal curve by sampling the specimens ahead of the notch root is given. Having such a curve, we can now try to develop a simple algorithm to link the experimental data with the notion of Damage. In this sense we can introduce an operational local Damage distribution function

$$D(x) = 1 - \frac{\tilde{\tilde{I}}(x)}{\tilde{I}_0} \tag{3}$$

where $\tilde{\tilde{I}}(x)$ is the X-ray intensity from the damage field and $\tilde{I}_0$ is the X-ray intensity from the undamaged one. In the same manner, we can introduce an operational total Damage degree, $\bar{D}$, and a corresponding process zone length x_d by the relation:

$$\bar{D} = \int_0^{x_d} D(x)dx = \int_0^{x_d} \left[1 - \frac{\tilde{\tilde{I}}(x)}{\tilde{I}_0}\right]dx \tag{4}$$

In Fig. 5 the experimental X-ray signal intensity curves for three specimens S1, S3 and S9 are given. These curves were obtained by means of a band-zone, slow scanning mode on the SEM-screen, as shown in the sketch of Fig. 4b. In this way the effective electron probe becomes a line (thickness about 1 μm) vertical to the notch length scans a region ahead of the notch root in form of a sampling band with a width equal to the notch root width. This mode of sampling was chosen to increase the efficiency of the measurements and to have a better average of the emitted information from the material. By these curves the actual damage or process zone length, x_d, can be measured as it is shown in Fig. 4a. As it was expected this length increases when cutting speed is increased, but by far not proportionally with this, i.e. increases much lower, from about 200 μm to about 300 μm and further to about 450 μm. At the same time we can introduce a

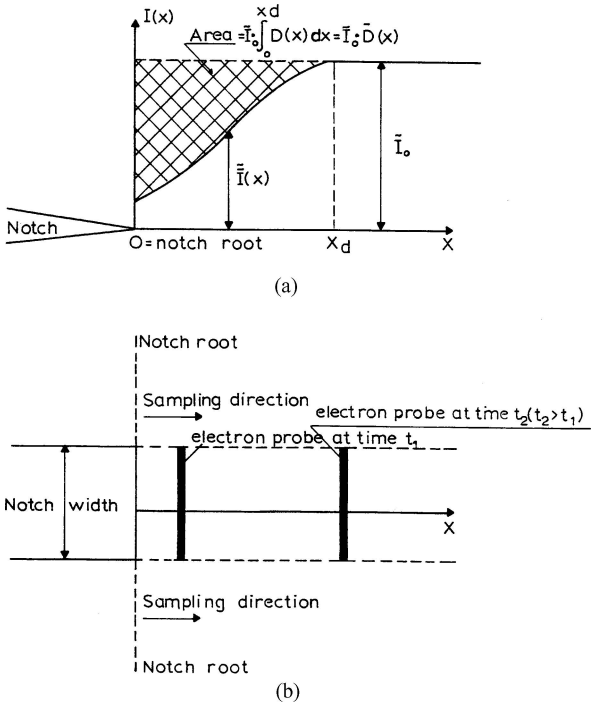

Figure 4 (a) Sketch of operative local damage distribution $(I(x) - \tilde{\tilde{I}}/(x))$ with associated total-average damage degree (dashed area) and process zone length x_d ahead of notch-tip. (b) Sampling geometry ahead of notch-tip: electron probe line is moving in direction "x" and is giving a continuous band-type geometry of sampling.

proportionality parameter q_p, given by the ratio of damage lengths which express the rate of growth of the process zones. Under condition of proportional increasing in cutting speeds, given by the value of proportionality $q_{v=3}$, and for the above measured damage zone lengths one obtain $q_p \cong 1{,}5$. Furthermore, from the shape of the curve in Fig. 5 the general form of the field of the local damage distribution and or its gradient (steepness) can be estimated.

It should be mentioned that despite relatively high noise in the signal, one can clearly see the signal curve formation from "zero" level and up to a limiting-constant one ("zero" level was chosen as a reference signal by convenient DC-offset control). In this sense the notch root region gives a minimum ("zero") signal while the region beyond the process zone length, x_d, gives a maximum limiting one.

Taking into consideration the average x-ray spatial resolution of the electron beam and the effective sampling geometry shown in Fig. 4b we have roughly estimated an effective local sampling volume of the order of 10^4–10^5 μm^3. This value is by far lower as those "imposed" by the local limiting approach of the continuum damage mechanics and which is of the order of 10^9 μm^3 in composites [6]. The second value is so high because the "size" of the volume in the damage mechanics has to be large enough in order to represent the local properties by their mean values through continuous variables. In this sense one can not talk of damage gradients below the second value (10^9 μm^3) since they have no macro-

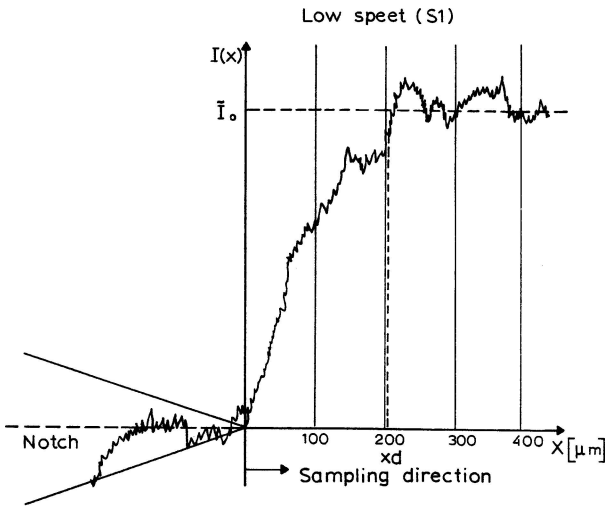

(a)

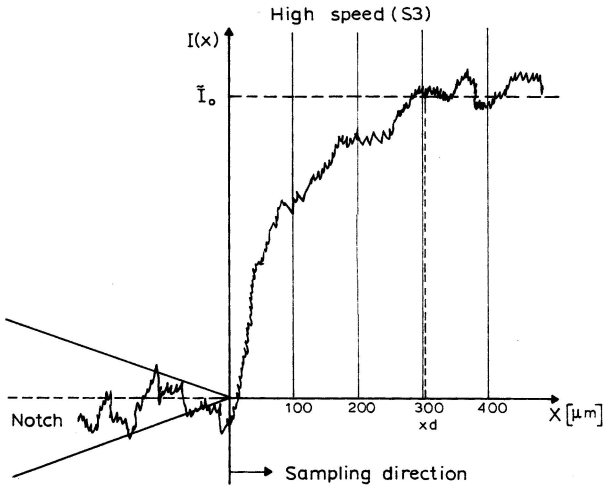

(b)

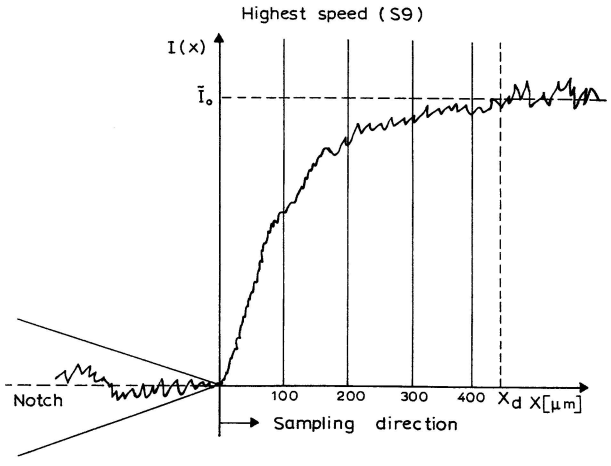

(c)

Figure 5 (a) X-ray measured operative local damage distribution for low operative damage level, *S*1, of induced damage. (b) X-ray measured operative local damage distribution for high operative damage level, *S*3, of induced damage. (c) X-ray measured operative local damage distribution for highest operative level, *S*9, of induced damage.

scopical physical sense, due to the heterogeneities of the material and of the nature of damage. Hence any theoretical modelling on the basis of damage mechanics to include the local damage distribution ("gradient") shown for example in the measurements of Fig. 5 cannot be accepted. At the same time bearing in mind the simplicity of the continuum mechanics and the physical foundation of the micromechanics [6, 8] which describes microcracks and pores on the mesoscale expressed by an assembly of grains, a promising strategy for such modelling would consist in combining the best features of both mechanics.

After smoothing the curves (averaging the noise) and in accordance with Equation 4 and by integrating the areas over the curves (dashed area in Fig. 4a), we can obtain the important relationship:

$$\frac{\bar{D}_3}{\bar{D}_1} \cong \frac{\bar{D}_9}{\bar{D}_3} \cong 1,2 = q_d < \frac{\upsilon_3}{\upsilon_1} = \frac{\upsilon_9}{\upsilon_3} = 3 = q_\upsilon \quad (\upsilon_9 = 3\upsilon_3 = 9\upsilon_1) \quad (5)$$

where indices 1, 3 and 9 correspond to the measured parameters of specimens S1, S3 and S9 respectively. The main resultant from all the above assessments is the fact that the two damage parameters q_d and q_p do not increase with the same rate as q_v increases (the damage degree having the lowest rate). Taking into account that the control parameter q_v is proportional to the increasing "cutting energy" it becomes evident that an appreciable part of this energy should be spent into other forms of energy dissipation such as frictional heat and/or abrasion (material loss) where frictional heat energy is assumed to be by far higher than the abrasion energy. Moreover the rotating disc-cutting procedure can be assumed to lead to a quasi-dynamic loading process at the forming notch. In this manner the induced micro-cracking or "quasi-spall" damage is due to quasi-impulsive compression shear by which the frictional forces are transmitted from the rotating disc to the notch-root material.

It is clear that the extent of the so induced "quasi-spall" damage, under the same testing conditions, depends to a high degree on the internal (residual) stresses due to the anisotropy of the elastic constants and the thermal expansion between the grains of the polycrystralline Alumina (Al_2O_3). Such internal stresses may be introduced during cooling from sintering or hot pressing temperature causing their dependence on the degree of thermal expansion anisotropy of the material. In the stress field ahead of the forming notch-root potential microcracking nuclei are activated by superposition with the above anisotropic thermal expansion stresses and in this way the earlier mentioned damage in form of intergranular microcracks can develop.

The relation (5) can be further interpreted in the following way: In the first approximation we can assume that $\upsilon \cong$ const. $\times$ (cutting energy $= E$), i.e. $\upsilon_1 \cong cE_1$, $\upsilon_3 \cong cE_3$, $\upsilon_9 = cE_9$ and $\upsilon_i = c \cdot E_i$. We can further

assume also in the first approximation that

$$\begin{aligned} E_1 &\cong E^{(1)}_{\mathrm{mcr}} + E^{(1)}_{\mathrm{mpl}} + E^{(1)}_h \\ E_3 &\cong E^{(3)}_{\mathrm{mcr}} + E^{(3)}_{\mathrm{mpl}} + E^{(3)}_h \\ E_9 &\cong E^{(9)}_{\mathrm{mcr}} + E^{(9)}_{\mathrm{mpl}} + E^{(9)}_h \\ &\cdots\cdots\cdots\cdots\cdots\cdots \\ E_i &\cong E^{(n)}_{\mathrm{mcr}} + E^{(n)}_{\mathrm{mpl}} + E^{(n)}_h \quad \text{with} \quad n = 3^i, \\ & \qquad\qquad\qquad\qquad (i = 0, 1, 2, \ldots) \end{aligned} \tag{6}$$

where E_{mcr} is the energy for micro-cracking, E_{mpl} is the energy for micro-plasticity and E_h is the heat energy, mainly by cutting friction. Further, we can assume for a ideal-brittle micro-cracking damage that

$$\bar{D}_i \propto E^{(i)}_{\mathrm{mcr}} \quad \text{and so} \quad E^{(i)}_{\mathrm{mpl}} << E^{(i)}_{\mathrm{mcr}} \tag{7}$$

Taking into consideration all of the above assumptions, we have

$$\frac{E^{(i)}_{\mathrm{mcr}}}{E^{(k)}_{\mathrm{mcr}}} = q_d < \frac{E^{(3n)}_{\mathrm{mcr}} + E^{(3n)}_h}{E^{(n)}_{\mathrm{mcr}} + E^{(n)}_h} \cong 3, \tag{8}$$

Because $E^{(i)}_h > E^{(k)}_h$ (higher cutting speeds means higher friction heat), the above relations (6) and (8) may be explained by means of energy dissipation due to increasing frictional heat between cutting tool and specimen material and due to micro-cracking.

Thereafter it can be mentioned that the energies $E^{(i)}_h$ might be roughly estimated by measuring the temperature increase of a cooling, small silicon oil bath beneath the rotating cutting disc. In this way the relation (8) may allow to evaluate experimentally the average micro-cracking damage energies ($E^{(i)}_{\mathrm{mcr}}$) for each specimen. Such experiments are conducted at present in the SEM-laboratory by the first two of the authors by taking a greater number of cutting speeds S*i* and porosities. At the same time the effects of the size of the specimen cutting surfaces on the frictional heat energies $E^{(\mathrm{i})}_h$ and microcracking energies $E^{(\mathrm{i})}_{\mathrm{mcr}}$ are investigated. We believe that the results reported in this study justify further experiments to establish the extent and reliability of the assumed correlations between the proposed damage parameters q_d, q_p and control parameter q_υ. It is hoped that, by making systematic quantitative measurements concerning surface roughness and impact energy, it will be possible to establish new qualitative as well as semi-quantitative relationships between micro- and macrofailure behaviour of the material in terms of its internal damage.

4. Conclusions

This study has shown that the two SEM-"subtechniques", electron fractography and X-ray EPMA, can be powerful tools for a combined experimental approach to qualitative and semi-quantitative correlations between micro-failure behaviour of the material and some of its microstructural and mechanical parameters such as degree of microcracking damage, porosity and loading rate. In this context the SEM-fractography has made, in an indirect way, evident the existence of the cutting-induced damage. This was possible by qualitative correlation of some characteristic fractographic features with well-known microfailure mechanisms. At the same time it was assumed that due to micromechanical interactions between internal pores and induced microcracks taking place during the cutting procedure, certain "combined-defect" sites are developed which in last instance should control the microfailure behaviour. One of the basic results obtained by this qualitative approach is the fact that for high porosity and for a given loading rate the induced damage by interaction with internal pores tends to lower the dissipation capability of the material concerning the fracture energy whereas for low level of porosity the induced damage tends to increase this capability. Loading rate effects were observed for material with low porosity where an increase in the rate tends to lower this capability. High porosity on the other hand by interaction with the induced damage shows no detectable loading rate effects on the microfailure behaviour of the material.

By means of the X-ray-EPMA technique and by implementation of a semi-quantitative experimental modelling approach it was possible to measure the local damage distribution and to evaluate the total (average) damage degree and the process zone size ahead of the notch root. It seems that the last two damage parameters can be controlled by the speed of the rotary cutting disc and in this instance this procedure might be useful, in a complementary way to the well-known "classical" microhardness indentation test, for material characterization in terms of internal damage. In the frame of the same methodology and by means of some simplifying assumptions, for example ideal brittle damage, a simple procedure for evaluation of the average microcracking damage energy was proposed.

References

1. A. G. EVANS and D. B. MARSHALL, *Acta Metall.* **37** (1989) 2567.
2. S. W. FREIMAN, *Amer. Cer. Soc. Bul.* **67**(2), (1988) 392.
3. G. D. QUINN, *J. Mat. Sci.* **22** (1986) 527.
4. H. NAYEB-HASHEMI and C. A. TRACY, *Exp. Mech.* (1991) 366.
5. K. TANAKA, *J. Mat. Sci.* **22**, (1987) 1501.
6. Continuum Damage Mechanics: Theory and Applications, edited by D. Krajcinovic and J. Lemaitre (Springer-Verlag, Wien-New York, 1987).
7. P. E. FLEWITT and R. K. WILD, Physical Methods for Materials Characterization#x200C; Institute of Physics Publishing, Bristol and Philadelphia (1994).
8. D. KRAJCINOVIC "Damage Mechanics", (Elsevier, Amsterdam, 1996).
9. Y. S. CHENG and Y. HUANG, *Eng. Fract. Mech.* **31**(6) (1988) 985.
10. J. LEMAITRE and J. DUFAILLY, *ibid.* **28** (1987) 643.
11. I. N. PRASSIANAKIS and E. N. THGEOTOKOGLOU, Proceedings of the 13th WCNDT, Sao Paolo, Brazil, 18-23 October, (Elsevier, Amsterdam, 1992), vol. II, 1054.

12. G. C. KNOLLMAN and R. C. YEE, *Exp. Mech.* **28**(2) (1988) 110.
13. K. L. POWELL, J. A. YEOMANS and P. A. SMITH, *J. Microscopy* **169**(2) (1993) 189.
14. G. A. BRIGGS, C. W. LAWRENCE and C. B. SERUBY, *ibid.* **169**(2) (1993) 139.
15. A. J. WINN, A. R. BOCCACCINI, N. IMAM and P. A. TRUSTY, *ibid.* **189**(1) (1997) 35.
16. V. R. SKALSKY, O. M. SERHIYENKO and O. YE. ANDREYKIV, Proceedings of ECF14, Fracture Mechanics Beyond 2000 Vol. III/III, edited by A. Neimitz, D. Rocach, D Kocanda and K. Golos, (EMAS. Publishing, 2002) p. 317.
17. D. VAVRIK, J. JAKUBEK, J. VISSAHERS, S. POSPISIL and J. ZEMANKOVA, in Proceedings of ECF14 Fracture Mechanics Beyond 2000 Vol. III/III, edited by A. Neimitz, D. Rocah, D. Kocanda and K. Golos (EMAS Publishing, 2002) p. 485.
18. H. P. DEGISCHER and A. SASOV, *European Microscopy and Analysis* **67** (September 2000) 37.
19. K. LINGA MURTY, K. DETEMPLE, O. KANERT, G. PETERS and J. TH. M. DEHOSSON, *J. Mat. Sci.* **31**(12) (1996) 3289.
20. R. W. RICE, *ibid.* **19**, (1984) 895.
21. P. POLUKHIN, S. GORELIK and V. VORONTSOV, "Physical Principles of Plastic Deformation", Engl. Translation (Mir Publishers, 1983).
22. J. I. GOLDSTEIN, D. E. NEWBURY, P. ECHLIN, D. C. JOY JR., A. D. ROMING, C. E. LYMAN, C. E. FIORI and E. LIFSHIN, "Scanning Electron Microscopy and *X*-ray Microanalysis" (Plenum Press, New York and London, 1992).
23. "Practical Scanning Electron Microscopy-Electron Probe and Ion Microprobe Analysis", edited by J. I. Goldstein and H. Yakowits (Plenum Press, New York and London, 1976).

Received 17 July 2003
and accepted 17 December 2004